

Article

# Nitrogen-Doped Graphene Quantum Dot-Passivated $\delta$ -Phase CsPbI<sub>3</sub>: A Water-Stable Photocatalytic Adjuvant to Degrade Rhodamine B

Yiting Gu, Xin Du, Feng Hua, Jianfeng Wen, Ming Li \* and Tao Tang \* 

College of Science & Key Laboratory of Low-Dimensional Structural Physics and Application, Education Department of Guangxi Zhuang Autonomous Region, Guilin University of Technology, Guilin 541004, China; yiting10596@163.com (Y.G.); duxin0727@126.com (X.D.); huafeng6026@163.com (F.H.); wjfulater@163.com (J.W.)

\* Correspondence: liming928@163.com (M.L.); tangtao@glut.edu.cn (T.T.)

**Abstract:** Inorganic halide perovskite CsPbI<sub>3</sub> is highly promising in the photocatalytic field for its strong absorption of UV and visible light. Among the crystal phases of CsPbI<sub>3</sub>, the  $\delta$ -phase as the most aqueous stability; however, directly using it in water is still not applicable, thus limiting its dye photodegradation applications in aqueous solutions. Via adopting nitrogen-doped graphene quantum dots (NGQDs) as surfactants to prepare  $\delta$ -phase CsPbI<sub>3</sub> nanocrystals, we obtained a water-stable material, NGQDs-CsPbI<sub>3</sub>. Such a material can be well dispersed in water for a month without obvious deterioration. High-resolution transmission electron microscopy and X-ray diffractometer characterizations showed that NGQDs-CsPbI<sub>3</sub> is also a  $\delta$ -phase CsPbI<sub>3</sub> after NGQD coating. The ultraviolet-visible absorption spectra indicated that compared to  $\delta$ -CsPbI<sub>3</sub>, NGQDs-CsPbI<sub>3</sub> has an obvious absorption enhancement of visible light, especially near the wavelength around 521 nm. The good dispersity and improved visible-light absorption of NGQDs-CsPbI<sub>3</sub> benefit their aqueous photocatalytic applications. NGQDs-CsPbI<sub>3</sub> alone can photodegrade 67% rhodamine B (RhB) in water, while after compositing with TiO<sub>2</sub>, NGQDs-CsPbI<sub>3</sub>/TiO<sub>2</sub> exhibits excellent visible-light photocatalytic ability, namely, it photodegraded 96% RhB in 4 h. The strong absorption of NGQDs-CsPbI<sub>3</sub> in the visible region and effective transfer of photogenerated carriers from NGQDs-CsPbI<sub>3</sub> to TiO<sub>2</sub> play the key roles in dye photodegradation. We highlight NGQDs-CsPbI<sub>3</sub> as a water-stable halide perovskite material and effective photocatalytic adjuvant.

**Keywords:** nitrogen doping; graphene quantum dot; perovskite; photodegradation



**Citation:** Gu, Y.; Du, X.; Hua, F.; Wen, J.; Li, M.; Tang, T. Nitrogen-Doped Graphene Quantum Dot-Passivated  $\delta$ -Phase CsPbI<sub>3</sub>: A Water-Stable Photocatalytic Adjuvant to Degrade Rhodamine B. *Molecules* **2023**, *28*, 7310. <https://doi.org/10.3390/molecules28217310>

Academic Editor: Sergio Navalon

Received: 24 September 2023

Revised: 22 October 2023

Accepted: 26 October 2023

Published: 28 October 2023



**Copyright:** © 2023 by the authors. Licensee MDPI, Basel, Switzerland. This article is an open access article distributed under the terms and conditions of the Creative Commons Attribution (CC BY) license (<https://creativecommons.org/licenses/by/4.0/>).

## 1. Introduction

In recent years, with the rapid development of the economy and technology, organic dyes have been widely used and discharged into industrial wastewater. Especially, rhodamine B (RhB), which is widely used for dyeing fabrics, paints, acrylics, and biological products, has become abundant in wastewater and highly toxic to organisms [1]. Previous studies have shown that RhB can induce growth retardation and liver damage, erythrocyte hemolysis, and suppression of the immune response in isolated spleen cells [2]. Other studies have suggested that RhB is mutagenic and carcinogenic [3] and could produce local sarcomas [2]. Therefore, it is urgent to develop economic and effective ways to remove RhB in wastewater. Producing highly oxidative active species is the basic technique for removing organic pollutants. Photocatalysis is a feasible and economic way to produce oxidative species and has been widely studied [4–6]. Fujishima and Honda first reported the photocatalytic performance of TiO<sub>2</sub> [7], and since then many scholars have investigated its photodegradation effect [8,9]. However, its wide band gap of 3.2 eV determines that only UV light can be absorbed, and visible light, the main component of sunlight, cannot be well captured by TiO<sub>2</sub> [10]. To obtain a visible-light photocatalyst, one way is to choose

a photocatalytic material with a narrower band gap. Typically, graphitic  $C_3N_4$ , with a band gap of  $\sim 2.71$  eV, can absorb visible light and has been proven effective in visible-light photodegradation [11], but the high carrier recombination rate remarkably restrains its photocatalytic performance [12]. The other way is compositing a visible-light responsive photocatalytic adjuvant with  $TiO_2$ , which turns visible light into photogenerated carriers and effectively transfers them to  $TiO_2$ , and then charged oxidative species are produced to degrade organic dyes. Carbon-based materials are universal adjuvants due to their widely tunable bandgaps, ease of composition, good aqueous dispersibility, and availability of carrier separation and transfer [13–16]. However, carbon-based materials suffer from weak visible-light absorption ability because their absorption mainly comes from the energy transition from  $\sigma$  or  $\pi$  to  $\pi^*$  orbitals [17]. Searching for an alternative adjuvant with strong absorption in the visible region is beneficial to improving the visible-light photocatalytic performance of  $TiO_2$ .

Halide perovskite, the rising star in optoelectronics, has been successfully applied in photocatalytic fields such as carbon dioxide reduction [18], water splitting [19], and dye removal [20]. Its strong visible-light acquisition ability plays the key role in photocatalysis. However, poor water stability generally is the Achilles heel of halide perovskite, so such experiments have to be conducted in organic solvents or after water-resistant coating [18–20]. With the invasion of water, the perovskite structure tends to stretch, distort, and tilt, turning  $\alpha$ -,  $\beta$ -, and  $\gamma$ -phases into  $\delta$ -phase [21].  $\delta$ -phase halide perovskite is generally deemed as a waste phase because it no longer exhibits typical perovskite characteristics, for example, strong photoluminescence (PL) and high quantum yield (QY) [22,23]. Also, because of this,  $\delta$ -phase perovskite is the most water stable, and the low PLQY means very few photogenerated carriers undergo direct recombination. Both of these properties are very suitable for aqueous photocatalysis.

Herein, we studied the photodegradation performance of  $\delta$ - $CsPbI_3$  nanocrystals on RhB. The  $\delta$ - $CsPbI_3$  nanocrystals synthesized by the conventional method using oleic acid and oleylamine as surfactants tend to aggregate and cannot be well dispersed in water, so it is hard to perform photodegradation experiments. By using nitrogen-doped graphene quantum dots (NGQDs) as surfactants to synthesize  $\delta$ -phase  $CsPbI_3$  [24], we obtained NGQDs- $CsPbI_3$ , which could be perfectly dispersed and stably stored in water for a month. After compositing with  $TiO_2$ , under visible light, the photogenerated electrons in NGQDs- $CsPbI_3$  transfer to  $TiO_2$ , producing the oxidant radicals  $\bullet O_2^-$  and  $\bullet OH$ , and the photogenerated holes left in NGQDs- $CsPbI_3$  combine with  $H_2O/OH^-$  to produce  $\bullet OH$ , finally oxidizing RhB into mineralization products. NGQDs- $CsPbI_3/TiO_2$  exhibits excellent visible-light photocatalytic ability, which could photodegrade 96% RhB in 4 h. As a water-stable material, NGQDs- $CsPbI_3$  shows bright prospects in photocatalysis, and it also opens the door to resurrecting the potential of  $\delta$ -phase halide perovskites.

## 2. Results

Typical TEM images of the synthesized samples are shown in Figure 1. The NGQDs are sized 1–10 nm [Figure S1a], with 65.09, 24.05, and 10.76 at.% of C, O, and N, respectively [Figure S1b]. Figure 1a shows a single NGQD of  $\sim 5$  nm with a lattice stripe distance of  $\sim 0.22$  nm, which is similar to that of graphite ( $11\bar{2}0$ ) facets [25]. The  $\delta$ -phase  $CsPbI_3$  nanocrystals are sized 5–20 nm [Figure S2a]. A typical 5 nm nanocrystal is shown in Figure 1b, and the lattice stripes are clearly resolved with interplanar spacing of 0.33 nm, corresponding to (212) planes of orthorhombic  $\delta$ - $CsPbI_3$  [26]. The borders of NGQDs- $CsPbI_3$  crystals are extremely irregular [Figure 1c], and their sizes are observably enlarged, obviously ascribed to the outcome of adopting NGQDs as surfactants. Figure 1d shows a large-size NGQDs- $CsPbI_3$  microcrystal, and its atomic distribution can be clearly seen with interplanar spacing of 0.35 nm. Figure S2c,d shows two other NGQDs- $CsPbI_3$  nano- or microcrystals, for which different crystal spacings are exhibited. One possibility is that these spacings correspond to different crystal planes of  $\delta$ - $CsPbI_3$ , and another is that the crystal structures of NGQDs- $CsPbI_3$  are miscellaneous since nonstoichiometric NGQDs

might bring about different strains to build  $\delta$ -CsPbI<sub>3</sub> with different crystal constants [27]. Among the large particles of TiO<sub>2</sub>, the NGQDs-CsPbI<sub>3</sub> crystals can also be resolved [see the yellow circle in Figure 1e]. From the crystal plane distance of 0.35 nm, one can know it is a NGQDs-CsPbI<sub>3</sub> nanocrystal [Figure 1f].

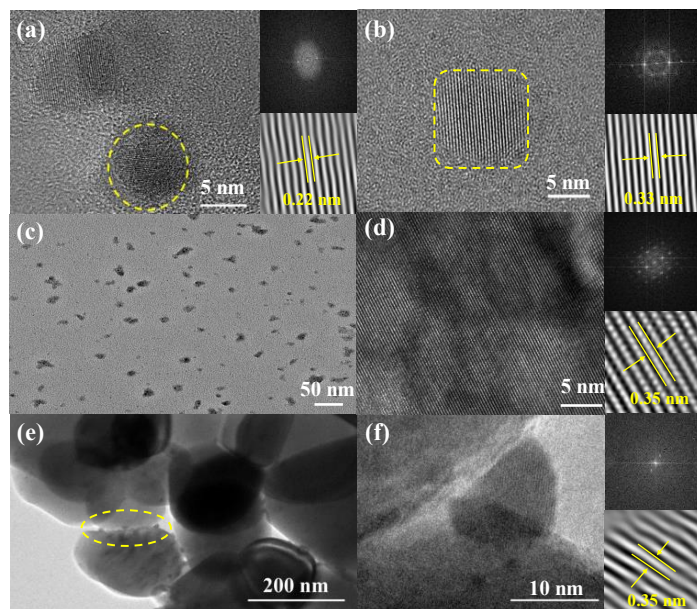


**Figure 1.** High-resolution TEM images of (a) NGQDs and (b)  $\delta$ -CsPbI<sub>3</sub>. (c) Large-scale and (d) high-resolution TEM images of NGQDs-CsPbI<sub>3</sub>. (e) Large-scale and (f) high-resolution TEM images of NGQDs-CsPbI<sub>3</sub>/TiO<sub>2</sub>. The lattice diagrams are the corresponding SAED patterns.

The EDS elemental mapping of an NGQDs-CsPbI<sub>3</sub> microcrystal is shown in Figure 2. Typical elements of NGQDs-CsPbI<sub>3</sub>, such as Cs, Pb, I, C, and N, can be found uniformly distributed. From Figure S3, one can know the atomic ratio of Cs:Pb:I  $\approx$  1:1:3, according to the formula of halide perovskite. The atomic ratio of Cs:C is  $\sim$ 1:8, and it must be stressed that the NGQD portion in NGQDs-CsPbI<sub>3</sub> may be overrated since NGQDs are used as surfactants and attached on the CsPbI<sub>3</sub> surface.

The XRD patterns are shown in Figure 3a. The prominent peaks of  $\delta$ -CsPbI<sub>3</sub> are (002), (102), (200), (201), (111), (112), (210), (113), (212), and (302) at 10.27°, 13.43°, 17.42°, 18.20°, 21.41°, 23.27°, 25.70°, 26.03°, and 27.55°, respectively, which are totally in accordance with the standard PDF25-0744 of orthorhombic  $\delta$ -phase CsPbI<sub>3</sub> [28]. NGQDs-CsPbI<sub>3</sub> exhibits similar characteristics, and in its XRD plot, the typical (002) peak of NGQDs is found at around 26° and is not well resolved [29]. Although some peaks are inconspicuous, NGQDs-CsPbI<sub>3</sub> can still be reasonably seen as orthorhombic  $\delta$ -phase CsPbI<sub>3</sub> with NGQDs on the surface. The XRD pattern of NGQDs-CsPbI<sub>3</sub>/TiO<sub>2</sub> [Figure 3b] demonstrates no new peaks aside from those of NGQDs-CsPbI<sub>3</sub> and TiO<sub>2</sub>, meaning that the two parts are merely physically composited.

The aqueous stability of the photocatalyst is a key factor on deciding whether it can be used in water to photodegrade organic dyes. In Figure 4a, one can find that the newly synthesized  $\delta$ -CsPbI<sub>3</sub> nanocrystals can be well dispersed in water; however, shortly after preparation, they are inclined to aggregate and hard to redisperse even with stirring, so  $\delta$ -CsPbI<sub>3</sub> nanocrystals are hardly used as aqueous photocatalysts. On the contrary, NGQDs-CsPbI<sub>3</sub> crystals could be well dispersed for a month, which is obviously highly related to the good dispersibility of NGQDs in water [30]. Here, we highlight the effect of nitrogen doping in enhancing dispersion, since we replaced NGQDs with graphene quantum dots (GQDs) to prepare GQDs-CsPbI<sub>3</sub> under the same conditions and found that, totally like  $\delta$ -CsPbI<sub>3</sub>, GQDs-CsPbI<sub>3</sub> tended to aggregate quickly. In Figure 4b, after 30 days, the PL shapes and intensities of NGQDs-CsPbI<sub>3</sub> nanocrystals change very slightly, demonstrating the water

stability of NGQDs-CsPbI<sub>3</sub>. It can also be found that the PL peak of NGQDs-CsPbI<sub>3</sub> can be deconvoluted into two parts: one is ascribed to NGQDs centered at 461 nm, and the other is ascribed to  $\delta$ -CsPbI<sub>3</sub> centered at 521 nm. The  $\delta$ -CsPbI<sub>3</sub> part demonstrates the typical green light of  $\delta$ -phase iodide perovskite, corresponding to self-trapped exciton emission [31]. In Figure 4c, via Tauc plotting, one can find that the bandgap of NGQDs-CsPbI<sub>3</sub> (3.09 eV) is a bit larger than that of  $\delta$ -CsPbI<sub>3</sub> (2.8 eV); however, in the visible region, especially around 521 nm, the absorption of NGQDs-CsPbI<sub>3</sub> is obviously stronger. Such absorption is ascribed to the transition from the ground states to trap states, namely, passivation through NGQDs can enhance the trapping exciton absorption of  $\delta$ -CsPbI<sub>3</sub>. The improvement in visible-light absorption undoubtedly benefits the photocatalytic ability of NGQDs-CsPbI<sub>3</sub>.

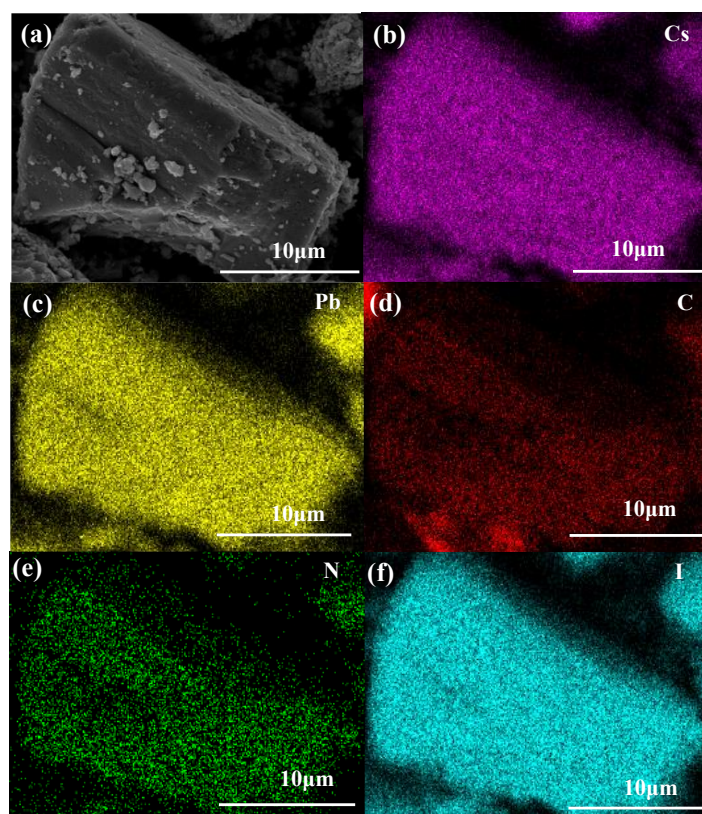


**Figure 2.** (a) SEM image of NGQDs-CsPbI<sub>3</sub> microcrystal and EDS elemental mapping of (b) Cs L, (c) Pb L, (d) C K, (e) N K, and (f) I L.

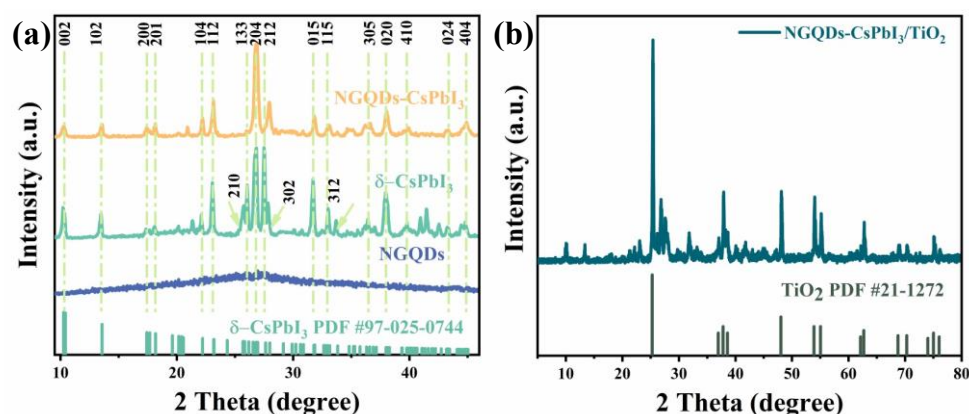


**Figure 3.** (a) XRD patterns of NGQDs,  $\delta$ -CsPbI<sub>3</sub>, and NGQDs-CsPbI<sub>3</sub>. (b) XRD pattern of NGQDs-CsPbI<sub>3</sub>/TiO<sub>2</sub>.

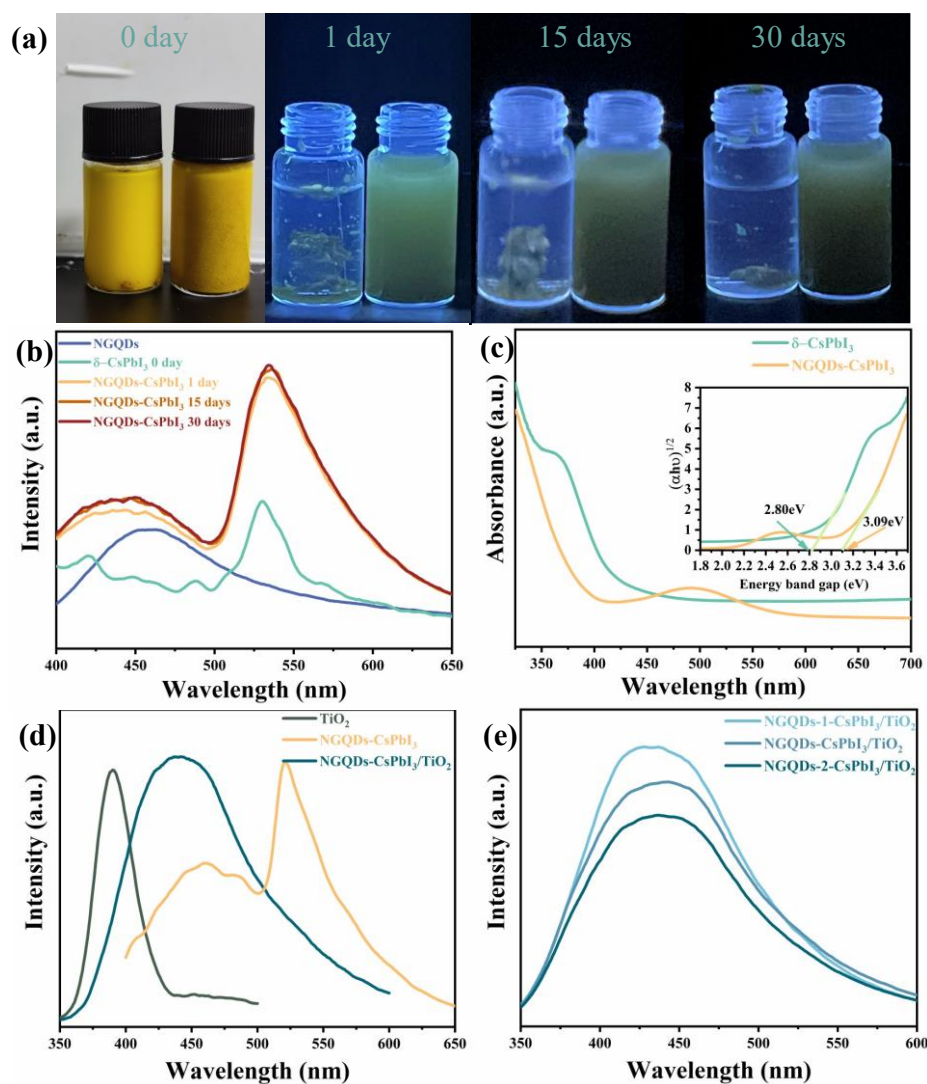


**Figure 4.** (a) Optical images under sun and UV light of  $\delta$ -CsPbI<sub>3</sub> (left) and NGQDs-CsPbI<sub>3</sub> (right) nanocrystals in water. (b) Time-dependent PLs of NGQDs-CsPbI<sub>3</sub>. (c) The absorption spectra of  $\delta$ -CsPbI<sub>3</sub> and NGQDs-CsPbI<sub>3</sub>. (d) The PLs of NGQDs-CsPbI<sub>3</sub> before and after compositing with TiO<sub>2</sub>. (e) The PLs of NGQDs-CsPbI<sub>3</sub>/TiO<sub>2</sub> with different NGQD mass ratios. The excitation wavelength is 330 nm.

Figure 4d shows the PLs of TiO<sub>2</sub> and NGQDs-CsPbI<sub>3</sub> before and after compositing. In the PL spectrum of NGQDs-CsPbI<sub>3</sub>/TiO<sub>2</sub>, the subpeak ascribed to  $\delta$ -CsPbI<sub>3</sub> (centered at 521 nm) is almost quenched, and the PL of TiO<sub>2</sub> (centered at 385 nm) is also invisible. NGQDs-CsPbI<sub>3</sub>/TiO<sub>2</sub> emits light with a single peak centered at ~440 nm, representing the characteristics of NGQDs, since it only exhibits a slight blue-shift compared to NGQDs alone (~460 nm). Therefore, we can speculate that the photogenerated electrons or holes in TiO<sub>2</sub> and CsPbI<sub>3</sub> are effectively transferred, and some of them recombine on NGQDs, namely on the coating surface of NGQDs-CsPbI<sub>3</sub> crystals. In Figure 4e, by tuning the NGQD mass ratio in NGQDs-CsPbI<sub>3</sub> (the NGQD mass is 0.5, 0.7, and 0.9 mg in NGQDs-1-CsPbI<sub>3</sub>, NGQDs-CsPbI<sub>3</sub>, and NGQDs-2-CsPbI<sub>3</sub>, respectively, and the CsPbI<sub>3</sub> mass is 72 mg), it is found that the PL positions remain invariable, merely along with slightly increased PL intensity due to the increase in NGQD weight. In a word, by compositing NGQDs-CsPbI<sub>3</sub> with TiO<sub>2</sub>, the photoinduced carriers in both can be effectively separated and transferred, which is highly beneficial to photocatalytic applications [32].

Taking 100 mL RhB water solution (10 mg/L) as a reference, we studied the visible-light ( $\lambda > 420$  nm) photodegradation activities of NGQDs-CsPbI<sub>3</sub>/TiO<sub>2</sub> (72.7 mg/250 mg). The effects of TiO<sub>2</sub> (250 mg), NGQDs (7 mg), NGQDs/TiO<sub>2</sub> (7 mg/250 mg), and NGQDs-CsPbI<sub>3</sub> (72.7 mg) are also supplied for comparison. The photodegradation results are shown in Figure 5a, where  $C_0$  and  $C$  are the initial and real-time concentrations of RhB, respectively, and  $C/C_0$  is determined by the absorbance of RhB at 554 nm. Due to the bad dispersibility of  $\delta$ -CsPbI<sub>3</sub>, it was hard to assess its photodegradation ability, so the related results are not shown here.

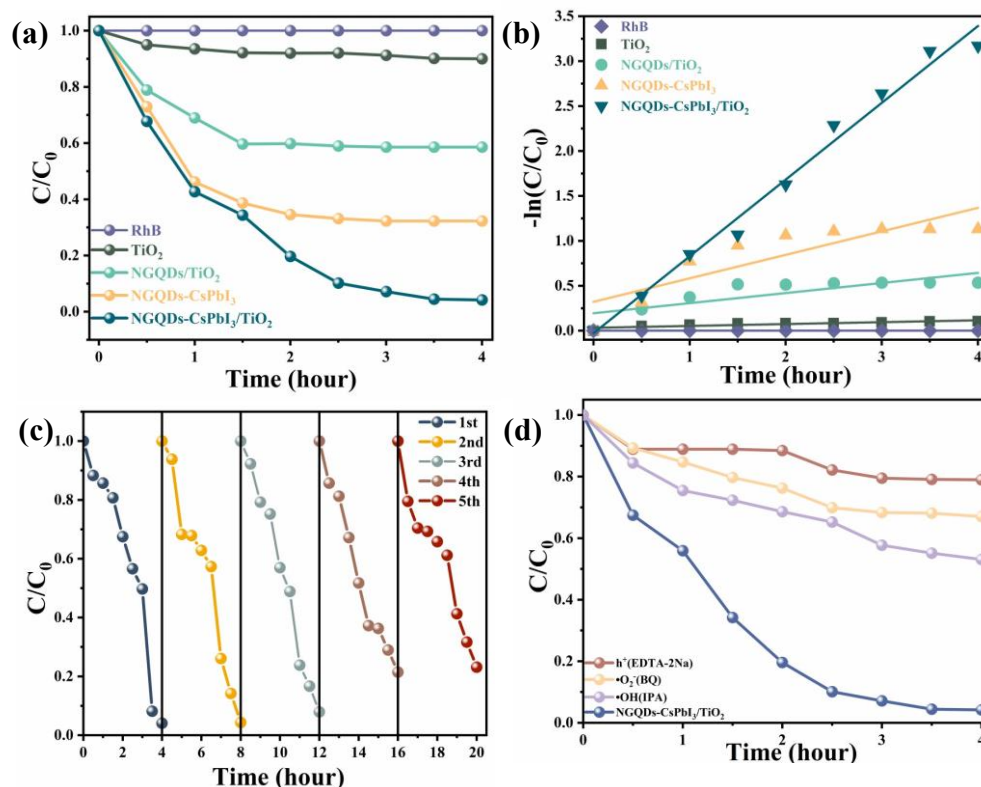


**Figure 5.** (a) Effects of different samples on the photocatalytic degradation of RhB under visible light (Xe lamp). (b) The corresponding degradation kinetic behaviors. (c) Photocatalytic cycle tests of NGQDs-CsPbI<sub>3</sub>/TiO<sub>2</sub>. (d) Effects of scavengers on the catalytic effect of NGQDs-CsPbI<sub>3</sub>/TiO<sub>2</sub>.

Obviously, the visible-light photocatalytic ability of TiO<sub>2</sub> or NGQDs alone is negligible, and the RhB photodegradation ratio is enhanced after compositing [30]. It is worth noting that NGQDs-CsPbI<sub>3</sub> alone displays decent photocatalytic activity, degrading 67% RhB in 4 h (see Section 4.4 for the calculation of photodegradation efficiency). The PLQY of NGQDs-CsPbI<sub>3</sub> is ~3% (Table S1) and together with its broad absorption range [Figure 4c], many indirect recombined photogenerated carriers can effectively participate in the photodegradation process. To further improve the photocatalytic activity, those photocarriers must be transferred to reduce the possibility of direct recombination. By compositing NGQDs-CsPbI<sub>3</sub> with TiO<sub>2</sub>, RhB can be nearly completely photodegraded (96%) after 4 h. Using total organic carbon (TOC) as a reference to measure the mineralization rate of RhB, similar photodegradation efficiency can be obtained, which is 94% in 4 h (Figure S4). Since the difference in photodegradation efficiency obtained by these two references (RhB absorbance and TOC) is small, all further discussion about the photodegradation of RhB is based on the former reference. The aforementioned discussion about Figure 4d shows that photocarriers are effectively transferred between TiO<sub>2</sub> and NGQDs-CsPbI<sub>3</sub> and TiO<sub>2</sub> is almost entirely inactive to visible light; hence, effective photocarrier transfer from NGQDs-CsPbI<sub>3</sub> to TiO<sub>2</sub> is the reason why the photodegradation activity can be im-

proved. The corresponding photodegradation kinetics were fitted using the first-order reaction equation:

$$\ln \frac{C}{C_0} = -kt \quad (1)$$

where  $k$  is the photocatalytic efficiency [33]. The  $k$  value of NGQDs-CsPbI<sub>3</sub>/TiO<sub>2</sub> is 0.85, almost 3 times that of NGQDs-CsPbI<sub>3</sub> alone [0.26, Figure 5b]. In order to further evaluate the usefulness of NGQDs-CsPbI<sub>3</sub>/TiO<sub>2</sub> nanocrystals as photocatalytic materials, cyclic experiments of RhB photodegradation were performed [Figure 5c]. Regrettably, a slight decrease in photodegradation activity appears in the 3rd to 5th cycles, with 92%, 79%, and 77%, respectively. This is due to the mass loss of NGQDs-CsPbI<sub>3</sub>/TiO<sub>2</sub>, especially NGQDs-CsPbI<sub>3</sub> nanocrystals, since it is difficult to completely collect nano-size particles in water through high-speed centrifugation. In Figure S5, one can find that using different ratios of NGQDs as surfactants to synthesize NGQDs-CsPbI<sub>3</sub> changes the photodegradation ability of NGQDs-CsPbI<sub>3</sub>/TiO<sub>2</sub>, and the optimal ratio is adopted in our experiments.

Generally, photogenerated •O<sub>2</sub><sup>−</sup>, holes (h<sup>+</sup>), and •OH play important roles in the degradation of organic dyes [34]. In order to identify which free radicals are dominant in photodegradation by NGQDs-CsPbI<sub>3</sub>/TiO<sub>2</sub>, radical capture experiments were conducted. As shown in Figure 5d, three scavengers, benzoquinone (BQ, 0.01 g/L), disodium ethylenediaminetetraacetate (EDTA-2Na, 0.02 g/L), and isopropyl alcohol (IPA, 0.02 g/L), were used in this study to capture the •O<sub>2</sub><sup>−</sup>, h<sup>+</sup>, and •OH radicals, respectively [35]. The RhB degradation rates of NGQDs-CsPbI<sub>3</sub>/TiO<sub>2</sub> nanocomposites were 21%, 33%, and 47% in the presence of EDTA-2Na, BQ, and IPA, respectively. The results showed that in our photocatalytic process, these three active components, •O<sub>2</sub><sup>−</sup>, •OH, and h<sup>+</sup>, are all massively produced and participate in dye oxidation, and the roles of •O<sub>2</sub><sup>−</sup> and h<sup>+</sup> are a bit more important than that of •OH. Regrettably, several capture agents (including AgNO<sub>3</sub>, K<sub>2</sub>Cr<sub>2</sub>O<sub>7</sub>, and KBrO<sub>3</sub>) were used to capture e<sup>−</sup>, and it was found that RhB was rapidly adsorbed and it was difficult to assess the photodegradation ability after e<sup>−</sup> capture.

In addition, Table 1 lists a comparison of relevant photocatalysts that have been used in several studies to degrade contaminants. Under visible light, the photodegradation ability of TiO<sub>2</sub> is negligible. Most halide perovskites can photodegrade dyes effectively, and these results show a good foreground of photocatalytic applications of perovskites. However, such experiments have been conducted in organic solution to ensure the stability of perovskites. As is known, the removal of organic contamination in wastewater is the first thing to be resolved; hence, to a certain degree, developing water-stable photocatalysts is more important than enhancing the photocatalytic efficiency alone. Obviously, NGQDs-CsPbI<sub>3</sub>/TiO<sub>2</sub> is a promising photocatalyst due to its feasibility of direct use in water, although there is much room for improvement in the photocatalytic efficiency.

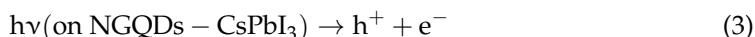
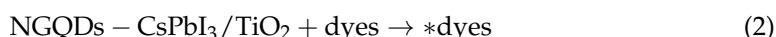
**Table 1.** Comparison of dye degradation effects of relevant photocatalysts under visible light.

No.	Catalysts	Dye Solution	Efficiency	Ref.
1	TiO <sub>2</sub>	RhB in water	10% in 4 h	[8]
2	CsPbBr <sub>3</sub>	RhB in toluene/ethanol	89% in 100 min	[36]
3	CsPbCl <sub>3</sub>	RhB in toluene/ethanol	90% in 100 min	[36]
4	Cs <sub>3</sub> AgInCl <sub>3</sub>	Sudan Red in ethanol	98.5% in 16 min	[20]
5	Cs <sub>4</sub> MnBiCl <sub>12</sub>	RhB in ethanol	97% in 7 min	[37]
6	Cs <sub>2</sub> AgBiBr <sub>6</sub> /Ti <sub>3</sub> C <sub>2</sub>	RhB in ethanol	100% in 70 min	[38]
7	NGQDs-CsPbI <sub>3</sub> /TiO <sub>2</sub>	RhB in water	96% in 4 h	our

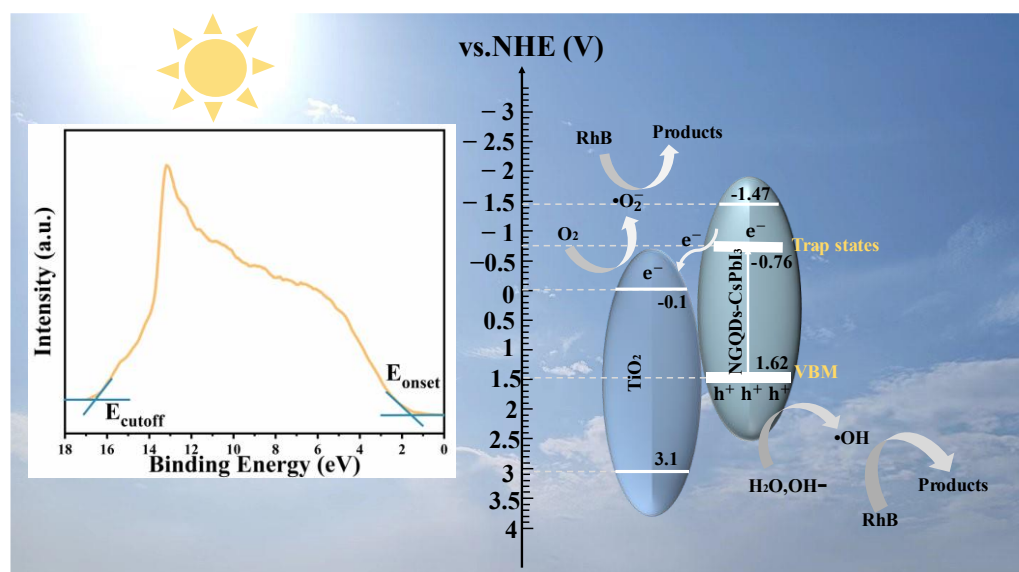
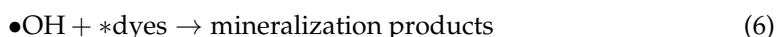
### 3. Discussion

Figure 6 shows a schematic diagram of the RhB photodegradation process of NGQDs-CsPbI<sub>3</sub>/TiO<sub>2</sub>. Using the vacuum level as a reference, the UPS measurement [inset of Figure 6] can define the valence band maximum (VBM) by  $E_{VBM} = -[21.22 - (E_{cutoff} - E_{onset})]$ . For NGQDs-CsPbI<sub>3</sub>, the  $E_{cutoff}$  is 16.53 eV and the  $E_{onset}$  is 1.59 eV, so the  $E_{VBM}$  is −6.12 eV. Considering the band gap is 3.09 eV, we know that the maximum conduction band (CBM)

is  $-3.03$  eV. The emissive center is located at  $521$  nm, implying that the energy difference between the trap states and VBM is  $2.38$  eV, namely, the energy level of the trap states is  $-3.74$  eV. Conventionally, we express energy levels using normal hydrogen electrode (NHE) as a reference [ $E(\text{NHE}) = -4.5 - E(\text{vacuum})$ , which represents the relationship between NHE and the vacuum energy levels], and the energy levels of CBM, the trap states, and VBM are  $-1.47$ ,  $-0.76$ , and  $1.62$  eV, respectively. The photocatalytic mechanism of NGQDs-CsPbI<sub>3</sub>/TiO<sub>2</sub> can be reasonably inferred according to the following expressions (2)–(8):



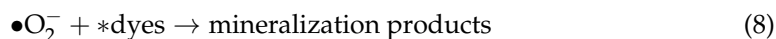
where \*dye denotes the dye molecules activated by NGQDs-CsPbI<sub>3</sub>/TiO<sub>2</sub>. When NGQDs-CsPbI<sub>3</sub>/TiO<sub>2</sub> is exposed to visible light, electrons and holes are only photogenerated in NGQDs-CsPbI<sub>3</sub> since TiO<sub>2</sub> is inactive under visible light. It also must be stressed that the electrons in NGQDs-CsPbI<sub>3</sub> can only be excited from VBM to the trap states since the photon energy ( $\lambda > 420$  nm) cannot compensate for the bandgap of NGQDs-CsPbI<sub>3</sub> ( $3.09$  eV). The primary function process of  $\bullet\text{OH}$  radicals is shown as the following expressions (4)–(6):



**Figure 6.** Mechanism of the photocatalytic process of NGQDs-CsPbI<sub>3</sub>/TiO<sub>2</sub>, and the inset is the UPS spectra of NGQDs-CsPbI<sub>3</sub>.

As shown in Figure 6, the photogenerated holes in NGQDs-CsPbI<sub>3</sub> combine with OH<sup>−</sup> generated by water to form  $\bullet\text{OH}$ , and then  $\bullet\text{OH}$  reacts with \*dyes to produce mineralization products. Generally speaking, oxidizing OH<sup>−</sup> into  $\bullet\text{OH}$  requires the holes to have a high potential. For example, in TiO<sub>2</sub> [39], Bi-doped LaFeO<sub>3</sub> [40], and g-C<sub>3</sub>N<sub>4</sub> [41], the hole potentials are 1.83, 1.97, and 1.84 V, respectively. However, in halide perovskite, this potential can decrease to as low as 1.1 V [36]. The VBM of NGQDs-CsPbI<sub>3</sub> is 1.62 eV, which might be enough for holes to generate  $\bullet\text{OH}$  radicals in such a perovskite material. Moreover, the broad PL and wide absorption of NGQDs-CsPbI<sub>3</sub> indicate that the excited electrons and holes are distributed in a wide energy range, which means the potentials

of many holes are higher than 1.62 V, further boosting the oxidation of  $\text{OH}^-$  into  $\bullet\text{OH}$  to degrade pollutants. The photodegradation process of  $\bullet\text{O}_2^-$  radicals can also be seen in Figure 6, as follows:



The electrons produced by photoexcitation are transferred from the trap states of NGQDs-CsPbI<sub>3</sub> to the CBM of TiO<sub>2</sub>, combine with the adsorbed O<sub>2</sub> to form  $\bullet\text{O}_2^-$ , and then  $\bullet\text{O}_2^-$  reacts with \*dyes to form mineralized compounds. Certainly, some  $\bullet\text{O}_2^-$  can be captured by H<sub>2</sub>O<sub>2</sub> to form  $\bullet\text{OH}$ , and again,  $\bullet\text{OH}$  reacts with \*dyes to form mineralized products.

## 4. Materials and Methods

### 4.1. Materials

Citric acid (CA, anhydrous), urea (99.5%), cesium iodide (CsI, 99.9%), oleylamine (OLA, 96%), dimethylformamide (DMF, 99.8%), and RhB (98%) were purchased from Shanghai Aladdin Biochemical Technology Co., Ltd. (Shanghai, China). Lead iodide (PbI<sub>2</sub>, 99.998%) was purchased from Alfa. Oleic acid (OA, 90%), P25 TiO<sub>2</sub> (80% anatase and 20% rutile), isopropyl alcohol (IPA), p-benzoquinone (BQ), and disodium EDTA-2Na were purchased from Xilong Chemical Co., Ltd. (Shantou, China). All chemicals were used directly without further purification.

### 4.2. Sample Synthesis

#### 4.2.1. Synthesis of NGQDs

First, 0.53 g CA and 0.6 g urea were dissolved in 12 mL deionized water and stirred to form a clarified solution. The solution was then transferred to a 50 mL Teflon autoclave. The sealed autoclave was heated to 160 °C in an oven and maintained for 8 h. The final product was collected by adding ethanol to the solution and centrifuging at 5000 rpm for 5 min. Finally, the sediment was dried at 60 °C to obtain NGQDs.

#### 4.2.2. Synthesis of $\delta$ -CsPbI<sub>3</sub>

First, 0.26 g CsI and 0.46 g PbI<sub>2</sub> were dissolved in 2 mL DMF, and the solution was heated to 50 °C and held at this temperature for 20 min. Subsequently, 0.4 mL OA and 0.2 mL OLA were added to stabilize the precursor solution, and then the precursor solution was heated to 90 °C and held at this temperature for 30 min. Finally, 0.2 mL precursor solution was quickly added to 4 mL deionized water (under vigorous stirring); after drying,  $\delta$ -CsPbI<sub>3</sub> nanocrystals were obtained.

#### 4.2.3. Synthesis of NGQDs-CsPbI<sub>3</sub>

The synthesis process of NGQDs-CsPbI<sub>3</sub> was similar to that of  $\delta$ -CsPbI<sub>3</sub>, except that the organic ligands OA and OLA were replaced by NGQDs. First, 0.26 g CsI and 0.46 g PbI<sub>2</sub> were dissolved in 2 mL DMF. Next, 7 mg NGQDs was added to obtain a precursor solution. Then, 0.2 mL precursor solution was rapidly added to 4 mL of deionized water (under vigorous stirring) to immediately generate NGQDs-CsPbI<sub>3</sub> crystals. For comparison, the initial mass ratio of NGQDs was tuned to synthesize NGQDs-CsPbI<sub>3</sub>, and these were named as NGQDs-1-CsPbI<sub>3</sub> and NGQDs-2-CsPbI<sub>3</sub> with initial NGQD masses of 5 and 9 mg, respectively.

#### 4.2.4. Synthesis of NGQDs-CsPbI<sub>3</sub>/TiO<sub>2</sub>

First, 250 mg TiO<sub>2</sub> was added into the above NGQDs-CsPbI<sub>3</sub> solution (including 72.7 mg NGQDs-CsPbI<sub>3</sub>, and the mass of NGQDs is 0.7 mg) and uniformly mixed with stirring; after drying, NGQDs-CsPbI<sub>3</sub>/TiO<sub>2</sub> composite was obtained.

### 4.3. Characterization

The crystal structures were characterized using a Miniflex-600 X-ray diffractometer (XRD, JEOL, Tokyo, Japan). The morphologies were assessed using a field emission transmission electron microscope (TEM, JEM2100F, Tokyo, Japan) equipped with a selected area electron diffractometer (SAED) and a scanning electron microscope (SEM, TESCAN MIRA LMS, Brno, Czech Republic) equipped with an energy dispersive spectroscopy (EDS). Surface analyses were carried out with an Escalab-250XI X-ray photoelectron spectrometer (XPS) from Thermo Fisher Scientific (Waltham, MA, USA). Ultraviolet-visible (UV-vis) absorption spectra were obtained using a PerkinElmer Lambda 750. Photoluminescence (PL) spectra were determined using an Edinburgh FL/FS900 carry Eclipse (Cheadle, UK). UV photoelectron spectroscopy (UPS) measurements were performed on a photoelectron spectrometer (ESCALAB 250Xi) with a He I source of 21.22 eV.

### 4.4. Photodegradation Test

The photocatalytic activities were investigated by photodegrading RhB (100 mL, 10 mg/L) under a xenon lamp (PLS-SXE 300, 300 W,  $\lambda > 420$  nm). The adsorption–desorption equilibrium of RhB and photocatalysts was achieved after being stirred in the dark for 0.5 h. Every 0.5 h, 4 mL solution was taken out to determine its RhB concentration using a Lambda 950 UV-Vis spectrophotometer. The recycle photodegradation experiments were conducted by repeatedly collecting the photocatalysts via centrifugation and drying.

The concentration of RhB was measured by UV-vis spectrophotometry and the degradation efficiency of RhB was calculated as:

$$\text{degradation ratio (\%)} = \frac{C_0 - C}{C_0} \times 100 = \frac{A_0 - A}{A_0} \times 100 \quad (9)$$

where  $C_0$  and  $C$  are the initial and real-time concentrations of RhB, respectively; and  $A_0$  and  $A$  are the initial and real-time absorbance of RhB at 554 nm, respectively. The mineralization rate of RhB solutions was measured using a TOC analyzer (Shimadzu, TOC-L CPN, Tsushima, Japan). The photodegradation ratio was determined by the following formula:

$$\text{degradation ratio (\%)} = \frac{\text{TOC}_0 - \text{TOC}}{\text{TOC}_0} \times 100 \quad (10)$$

where  $\text{TOC}_0$  and  $\text{TOC}$  are respectively the initial and real-time TOC of RhB solution.

## 5. Conclusions

Water-stable NGQDs-CsPbI<sub>3</sub> halide perovskite was successfully prepared by the thermal injection method at room temperature. It exhibits typical characteristics of  $\delta$ -phase CsPbI<sub>3</sub>, namely strong absorption in the visible region and low PL QY. Due to the coating and passivation through NGQDs, such a material can be well dispersed and is stable in water for a month, hence it can effectively photodegrade RhB. After compositing with TiO<sub>2</sub>, the photodegradation ability is further improved because the photogenerated e-h pairs can be effectively separated and transferred. We highlight NGQDs-CsPbI<sub>3</sub> as a water-stable perovskite with great potential in the photocatalytic field.

**Supplementary Materials:** The following supporting information can be downloaded at: <https://www.mdpi.com/article/10.3390/molecules28217310/s1>, Figure S1. (a) TEM image of NGQDs. (b) Statistical size distribution of the prepared NGQDs. (c) XPS full spectrum of NGQDs. (d) High-resolution of N 1s and C 1s spectra of NGQDs. Figure S2. (a) TEM images of  $\delta$ -phase CsPbI<sub>3</sub> nanocrystals. (b) Statistical size distribution of the prepared  $\delta$ -phase CsPbI<sub>3</sub>. (c) and (d) High-resolution TEM images of NGQDs-CsPbI<sub>3</sub> with different space stripes. Figure S3. (a) EDS mapping and (b) the atomic proportion of NGQDs-CsPbI<sub>3</sub>. Figure S4. Comparison of the photodegradation ratios of RhB obtained by the absorbance (Abs) and total organic carbon (TOC) analysis of RhB solution. Figure S5. The RhB photodegradation activities of different NGQDs-CsPbI<sub>3</sub>/TiO<sub>2</sub> samples by tuning the initial NGQDs mass. The NGQDs mass is 0.5, 0.7 and 0.9 mg in NGQDs-1-CsPbI<sub>3</sub>,

NGQDs-CsPbI<sub>3</sub> and NGQDs-2-CsPbI<sub>3</sub>, respectively, and the CsPbI<sub>3</sub> part is 72 mg. The mass of TiO<sub>2</sub> is 250 mg. Table S1. Quantum yields of  $\delta$ -CsPbI<sub>3</sub>, NGQDs, NGQDs-CsPbI<sub>3</sub> and NGQDs-CsPbI<sub>3</sub>/TiO<sub>2</sub> using quinine sulfate as a reference.

**Author Contributions:** Formal analysis, Writing—original draft preparation, Data curation, Y.G.; Investigation, Y.G., X.D. and F.H.; Conceptualization, Software, J.W.; Methodology, X.D. and F.H.; Supervision, T.T. and M.L.; Visualization, Y.G. and T.T.; Resources, Validation, Writing—review and editing, Project administration, T.T.; Funding acquisition, T.T. All authors have read and agreed to the published version of the manuscript.

**Funding:** This work was financially supported by the Natural Science Foundation of Guangxi Zhuang Autonomous Region of China (2018GXNSFAA050014) and the Foundation of Guilin University of Technology (GLUTQD2002023).

**Institutional Review Board Statement:** Not applicable.

**Informed Consent Statement:** Not applicable.

**Data Availability Statement:** The data can be made available upon reasonable request.

**Conflicts of Interest:** The authors declare that the research was conducted in the absence of any commercial or financial relationships that could be construed as a potential conflict of interest.

**Sample Availability:** Not applicable.

## References

1. Xu, D.; Ma, H. Degradation of rhodamine B in water by ultrasound-assisted TiO<sub>2</sub> photocatalysis. *J. Clean. Prod.* **2021**, *313*, 127758.
2. Elliott, G.S.; Mason, R.W.; Edwards, I.R. Studies on the pharmacokinetics and mutagenic potential of rhodamine B. *J. Toxicol.-Clin. Toxic.* **1990**, *28*, 45–59.
3. Gupta, V.K.; Suhas, Ali, I.; Saini, V.K. Removal of rhodamine B, fast green, and methylene blue from wastewater using red mud, an aluminum industry waste. *Ind. Eng. Chem. Res.* **2004**, *43*, 1740–1747.
4. Liu, Y.; Cheng, M.; Liu, Z.; Zeng, G.; Zhong, H.; Chen, M.; Zhou, C.; Xiong, W.; Shao, B.; Song, B. Heterogeneous fenton-like catalyst for treatment of rhamnolipid-solubilized hexadecane wastewater. *Chemosphere* **2019**, *236*, 124387.
5. Liu, Y.; Huang, D.; Cheng, M.; Liu, Z.; Lai, C.; Zhang, C.; Zhou, C.; Xiong, W.; Qin, L.; Shao, B.; et al. Metal sulfide/MOF-based composites as visible-light-driven photocatalysts for enhanced hydrogen production from water splitting. *Coord. Chem. Rev.* **2020**, *409*, 213220.
6. Xiao, S.; Cheng, M.; Zhong, H.; Liu, Z.F.; Liu, Y.; Yang, X.; Liang, Q.H. Iron-mediated activation of persulfate and peroxymonosulfate in both homogeneous and heterogeneous ways: A review. *Chem. Eng. J.* **2020**, *384*, 123265.
7. Emin, S.; Singh, S.P.; Han, L.; Satoh, N.; Islam, A. Colloidal quantum dot solar cells. *Nat. Energy* **2011**, *85*, 1264–1282.
8. Khalid, N.R.; Mazia, U.; Tahir, M.B.; Niaz, N.A.; Javid, M.A. Photocatalytic degradation of RhB from an aqueous solution using Ag<sub>3</sub>PO<sub>4</sub>/N-TiO<sub>2</sub> heterostructure. *J. Mol. Liq.* **2020**, *313*, 113522.
9. Lin, X.; Li, Y.X. Preparation of TiO<sub>2</sub>/Ag BMIM Cl composites and their visible light photocatalytic properties for the degradation of rhodamine B. *Catalysts* **2021**, *11*, 661. [[CrossRef](#)]
10. Todescato, F.; Fortunati, I.; Gardin, S.; Garbin, E.; Collini, E.; Bozio, R.; Jasieniak, J.J.; Della Giustina, G.; Brusatin, G.; Toffanin, S.; et al. Soft-lithographed up-converted distributed feedback visible lasers based on CdSe-CdZnS-ZnS quantum dots. *Adv. Funct. Mater.* **2012**, *22*, 337–344. [[CrossRef](#)]
11. Guo, Z.; Ni, S.; Wu, H.; Wen, J.; Li, X.; Tang, T.; Li, M.; Liu, M. Designing nitrogen and phosphorus co-doped graphene quantum dots/g-C<sub>3</sub>N<sub>4</sub> heterojunction composites to enhance visible and ultraviolet photocatalytic activity. *Appl. Surf. Sci.* **2021**, *548*, 149211.
12. Liu, Y.; Zeng, X.; Hu, X.; Hu, J.; Wang, Z.; Yin, Y.; Sun, C.; Zhang, X. Two-dimensional g-C<sub>3</sub>N<sub>4</sub>/TiO<sub>2</sub> nanocomposites as vertical Z-scheme heterojunction for improved photocatalytic water disinfection. *Catal. Today* **2019**, *335*, 243–251.
13. Zhang, L.; Zhang, Q.; Xie, H.; Guo, J.; Lyu, H.; Li, Y.; Sun, Z.; Wang, H.; Guo, Z. Electrospun titania nanofibers segregated by graphene oxide for improved visible light photocatalysis. *Appl. Catal. B Environ.* **2017**, *201*, 470–478.
14. Li, K.; Xiong, J.; Chen, T.; Yan, L.; Dai, Y.; Song, D.; Lv, Y.; Zeng, Z. Preparation of graphene/TiO<sub>2</sub> composites by nonionic surfactant strategy and their simulated sunlight and visible light photocatalytic activity towards representative aqueous POPs degradation. *J. Hazard. Mater.* **2013**, *250–251*, 19–28.
15. Ioan-Alexandru, B.; John, B.; Kiem, G.N.; Tobias, H.; Muhammad Tariq, S.; Stuart, A.J.T.; Alistair, R.; David, J.M.; Nicholas, P.P.; Sabina Alexandra, N.; et al. Outstanding visible light photocatalysis using nano-TiO<sub>2</sub> hybrids with nitrogen-doped carbon quantum dots and/or reduced graphene oxide. *J. Mater. Chem. A* **2023**, *11*, 9791–9806.
16. Guo, Z.; Wu, H.; Li, M.; Tang, T.; Wen, J.; Li, X. Phosphorus-doped graphene quantum dots loaded on TiO<sub>2</sub> for enhanced photodegradation. *Appl. Surf. Sci.* **2020**, *526*, 146724.

17. Li, M.; Wu, W.; Ren, W.; Cheng, H.; Tang, N.; Zhong, W.; Du, Y. Synthesis and upconversion luminescence of N-doped graphene quantum dots. *Appl. Phys. Lett.* **2012**, *101*, 103107.
18. Pan, A.; Ma, X.; Huang, S.; Wu, Y.; Jia, M.; Shi, Y.; Liu, Y.; Wangyang, P.; He, L.; Liu, Y. CsPbBr<sub>3</sub> perovskite nanocrystal grown on MXene nanosheets for enhanced photoelectric detection and photocatalytic CO<sub>2</sub> reduction. *J. Phys. Chem. Lett.* **2019**, *10*, 6590–6597.
19. Nam, S.; Mai, C.T.K.; Oh, I. Ultrastable photoelectrodes for solar water splitting based on organic metal halide perovskite fabricated by lift-off process. *ACS Appl. Mater. Interfaces* **2018**, *10*, 14659–14664.
20. Li, K.; Li, S.; Zhang, W.; Shi, Z.; Wu, D.; Chen, X.; Lin, P.; Tian, Y.; Li, X. Highly-efficient and stable photocatalytic activity of lead-free Cs<sub>2</sub>AgInCl<sub>6</sub> double perovskite for organic pollutant degradation. *J. Colloid Interface Sci.* **2021**, *596*, 376–383.
21. Huang, Z.; Qin, H.; Wen, J.; Jiang, L.; Hu, G.; Li, M.; Chen, J.; Liu, F.; Tao, T. Observation of abnormal photoluminescence upon structural phase competence and transition-induced disorder of stable  $\alpha$ -FAPbI<sub>3</sub>. *Opt. Mater. Express* **2022**, *13*, 263–271.
22. Monroy, M.I.P.; Goldberg, I.; Elkhoully, K.; Georgitzikis, E.; Clinckemalie, L.; Croes, G.; Annavarapu, N.; Qiu, W.; Debroye, E.; Kuang, Y.; et al. All-evaporated, all-inorganic CsPbI<sub>3</sub> perovskite-based devices for broad-band photodetector and solar cell applications. *ACS Appl. Electron. Mater.* **2021**, *3*, 3023–3033.
23. Straus, D.B.; Guo, S.; Cava, R.J. Kinetically stable single crystals of perovskite-phase CsPbI<sub>3</sub>. *J. Am. Chem. Soc.* **2019**, *141*, 11435–11439. [[PubMed](#)]
24. Chen, B.; Liao, W.; Wu, C. High-stability CsPbI<sub>2</sub>Br<sub>2</sub> nanocrystal with nitrogen-doped graphene quantum dot/titanium dioxide for enhancing rhodamine B photocatalytic degradation under visible light. *J. Environ. Chem. Eng.* **2022**, *10*, 107534.
25. Far'ain Md Noor, N.; Saiful Badri, M.A.; Salleh, M.M.; Umar, A.A. Synthesis of white fluorescent pyrrolic nitrogen-doped graphene quantum dots. *Opt. Mater.* **2018**, *83*, 306–314.
26. Yin, Y.; Cheng, H.; Tian, W.; Wang, M.; Yin, Z.; Jin, S.; Bian, J. Self-assembled  $\delta$ -CsPbI<sub>3</sub> nanowires for stable white light emission. *ACS Appl. Nano Mater.* **2022**, *5*, 18879–18884.
27. Steele, J.A.; Jin, H.; Dovgaliuk, I.; Berger, R.F.; Braeckvelt, T.; Yuan, H.; Martin, C.; Solano, E.; Lejaeghere, K.; Rogge, S.M.J.; et al. Thermal nonequilibrium of strained black CsPbI<sub>3</sub> thin films. *Science* **2019**, *365*, 679–684.
28. Kundu, S.; Richtsmeier, D.; Hart, A.; Yeddu, V.; Song, Z.; Niu, G.; Thrithamarassery Gangadharan, D.; Dennis, E.; Tang, J.; Voznyy, O.; et al. Orthorhombic non-perovskite CsPbI<sub>3</sub> microwires for stable high-resolution X-ray detectors. *Adv. Opt. Mater.* **2022**, *10*, 2200516.
29. Qu, D.; Zheng, M.; Du, P.; Zhou, Y.; Zhang, L.; Li, D.; Tan, H.; Zhao, Z.; Xie, Z.; Sun, Z. Highly luminescent S, N co-doped graphene quantum dots with broad visible absorption bands for visible light photocatalysts. *Nanoscale* **2013**, *5*, 12272–12277.
30. Zhang, J.; Zhang, X.; Dong, S.; Zhou, X.; Dong, S. N-doped carbon quantum dots/TiO<sub>2</sub> hybrid composites with enhanced visible light driven photocatalytic activity toward dye wastewater degradation and mechanism insight. *J. Photochem. Photobiol. A* **2016**, *325*, 104–110.
31. Xu, J.; Wu, Y.; Li, Z.; Liu, X.; Cao, G.; Yao, J. Resistive switching in nonperovskite-phase CsPbI<sub>3</sub> film-based memory devices. *ACS Appl. Mater. Interfaces* **2020**, *12*, 9409–9420. [[PubMed](#)]
32. Yuan, G.; Feng, S.; Yang, Q.; Yi, F.; Li, X.; Yuan, Y.; Wang, C.; Yan, H. Promoting charge separation in a composite of  $\delta$ -CsPbI<sub>3</sub> and covalent organic frameworks. *J. Mater. Chem. C* **2023**, *11*, 7570–7574.
33. Sarkar, D.; Ghosh, C.K.; Mukherjee, S.; Chattopadhyay, K.K. Three dimensional Ag<sub>2</sub>O/TiO<sub>2</sub> Type-II (p-n) nanoheterojunctions for superior photocatalytic activity. *ACS Appl. Mater. Interfaces* **2013**, *5*, 331–337.
34. Zhang, W.; Xiong, J.; Li, J.; Daoud, W.A. Seed-assisted growth for low-temperature-processed all-inorganic CsPbI<sub>2</sub>Br<sub>2</sub> solar cells with efficiency over 10%. *Small* **2020**, *16*, 2001535. [[CrossRef](#)] [[PubMed](#)]
35. Yang, J.; Zhu, H.; Peng, Y.; Li, P.; Chen, S.; Yang, B.; Zhang, J. Photocatalytic performance and degradation pathway of rhodamine B with TS-1/C<sub>3</sub>N<sub>4</sub> composite under visible light. *Nanomaterials* **2020**, *10*, 756. [[CrossRef](#)] [[PubMed](#)]
36. Gao, G.; Xi, Q.; Zhou, H.; Zhao, Y.; Wu, C.; Wang, L.; Guo, P.; Xu, J. Novel inorganic perovskite quantum dots for photocatalysis. *Nanoscale* **2017**, *9*, 12032–12038.
37. Qi, X.; Zhang, F.; Chen, Z.; Chen, X.; Jia, M.; Ji, H.; Shi, Z. Hydrothermal synthesis of stable lead-free Cs<sub>4</sub>MnBi<sub>2</sub>Cl<sub>12</sub> perovskite single crystals for efficient photocatalytic degradation of organic pollutants. *J. Mater. Chem. C* **2023**, *11*, 3715–3725. [[CrossRef](#)]
38. Cheng, S.; Chen, X.; Wang, M.; Li, G.; Qi, X.; Tian, Y.; Jia, M.; Han, Y.; Wu, D.; Li, X.; et al. In-situ growth of Cs<sub>2</sub>AgBiBr<sub>6</sub> perovskite nanocrystals on Ti<sub>3</sub>C<sub>2</sub>T<sub>x</sub> MXene nanosheets for enhanced photocatalytic activity. *Appl. Surf. Sci.* **2023**, *621*, 156877.
39. Chen, B.; Lu, W.; Xu, P.; Yao, K. Potassium poly(heptazine imide) coupled with Ti<sub>3</sub>C<sub>2</sub> MXene-derived TiO<sub>2</sub> as a composite photocatalyst for efficient pollutant degradation. *ACS Omega* **2023**, *8*, 11397–11405.
40. Sun, Y.; Long, W.; Guo, Y.; Wei, R.; Wang, Y.; Zhang, J.; Hu, S. Degradation of pollutants by Bi-doped LaFeO<sub>3</sub>/CQDs/CN Z-scheme heterojunction photocatalysts and mechanism study. *Diam. Relat. Mater.* **2022**, *130*, 109555.
41. Preeyanga, M.; Vinesh, V.; Neppolian, B. Complete removal of tetracycline by sonophotocatalysis using ultrasound-assisted hierarchical graphitic carbon nitride nanorods with carbon vacancies. *Chemosphere* **2021**, *287*, 132379. [[PubMed](#)]

**Disclaimer/Publisher's Note:** The statements, opinions and data contained in all publications are solely those of the individual author(s) and contributor(s) and not of MDPI and/or the editor(s). MDPI and/or the editor(s) disclaim responsibility for any injury to people or property resulting from any ideas, methods, instructions or products referred to in the content.